京都大学学術情報リポジトリ
KURENAI 紅
Kyoto University Research Information Repository

京都大学
KYOTO UNIVERSITY

京都大学学術情報リポジトリ
KURENAI 紅
Kyoto University Research Information Repository

JOURNAL OF CHEMICAL PHYSICS | VOLUME 117, NUMBER 3 | 15 JULY 2002

Dissociative ionization of ICl studied by ion imaging spectroscopy

Hidetaka Yamada, Nori Taniguchi, and Masahiro Kawasaki[a)]
Department of Molecular Engineering, Kyoto University, Kyoto 606-8501, Japan

Yutaka Matsumi
Solar Terrestrial Environment Laboratory, Nagoya University, Toyokawa 442-8505, Japan

Robert J. Gordon[b)]
Department of Chemistry (m/c 111), University of Illinois at Chicago, Chicago, Illinois 60607-7061

The speed and angular distributions of I^+ ions, produced when ICl molecules were exposed to both ultraviolet and visible radiation at 304+608 nm, 355+608 nm, and 304+532 nm, were measured by velocity map imaging. An intense central feature in the I^+ images was observed to be very sensitive to the polarization of the ultraviolet light and is attributed to a dissociative ionization mechanism involving three-body fragmentation: $ICl + h\upsilon$ (visible) $+ 3h\upsilon$ (ultraviolet) $\rightarrow I^+ + Cl + e^-$. The effect of varying the delay between the visible and ultraviolet radiation on the I^+ images suggests that an intermediate gateway state of ICl reached by absorption of one photon of visible light mediates the transition to the superexcited dissociative ionization state. © *2002 American Institute of Physics.* [DOI: 10.1063/1.1484106]

I. INTRODUCTION

In conventional studies of photodissociation employing weak visible (VIS) or ultraviolet (UV) radiation, a molecule, *AB*, absorbs a single photon and dissociates on the lowest potential energy surface accessible within the Franck-Condon widow. If the photon is sufficiently energetic, however, the molecule may be excited to a neutral superexcited state, *AB****, which can then decay either by predissociation,
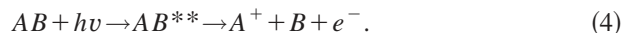
$$AB + h\upsilon \rightarrow AB^{**} \rightarrow A + B^*, \tag{1}$$
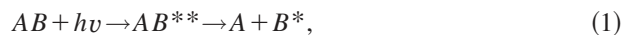
or by autoionization,

$$AB + h\upsilon \rightarrow AB^{**} \rightarrow AB^+ + e^-. \tag{2}$$
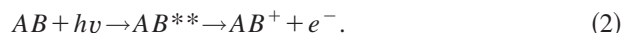
At energies close to ionization, excitation to ion-pair states may also be important,[1] i.e.,

$$AB + h\upsilon \rightarrow AB^{**} \rightarrow A^+ + B^-, \tag{3}$$
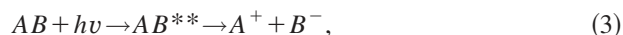
and if the ionic state is unbound, dissociative ionization (DI) may occur;

$$AB + h\upsilon \rightarrow AB^{**} \rightarrow A^+ + B + e^-. \tag{4}$$

The competition between photoionization and photodissociation is inherently interesting because it is typically a multielectron and multi-continuum process.[2]

Photoionization studies displaying these phenomena have been reported recently for I_2,[3] C_6H_5I,[4] H_3,[5] NO_2,[6] and CF_3I.[7] In the I_2 experiment[3] velocity map images of I^+ produced with VIS radiation between 556 and 576 nm displayed discrete anisotropic rings and a continuous central peak that were attributed to a multiphoton DI mechanism. The recoil energy associated with the discrete rings was independent of wavelength, indicating that the electron removed a variable amount of kinetic energy, leaving the nuclei on the same point of the repulsive potential energy curves for different initial excitation energies. At some wavelengths the anisotropy of the rings was diminished, and the recoil energy shifted to slightly larger values. Both of these effects could be explained by the presence of low-lying resonances or "gateway" states accessed by absorption of several VIS photons. The C_6H_5I experiment[4] was performed also using the velocity map imaging method, with radiation between 266 and 609 nm. Discrete rings and an hour-glass-shaped central feature were observed, and a multiphoton DI mechanism was proposed. Electron images produced at 532 nm are compatible with this mechanism; however, the complexity of the phenyl ring precludes an unequivocal interpretation of the data. A DI mechanism has also been proposed by Bakker *et al.*[5] for the single-photon ionization of the *E,F* states of H_2. From the angular distribution of the H^+ ions, they assigned the electronic transitions to the states that are responsible for the DI process.

The diatomic interhalogen molecules have been a subject of great interest from both experimental and theoretical points of view, not least because of the many curve crossings and avoided crossings among the excited state potential energy curves.[8] The rich manifold of low-lying electronic states is likely to play an important role in multiphoton processes including DI. We report here the results of a two-color, photofragment ion imaging study of the DI of iodine monochloride (ICl). One or more VIS photons excite an intermediate "gateway" state, and several UV photons access the ionization continuum. The use of two independent excitation sources allows us to separate the roles played by the intermediate state and the superexcited DI state. Variation of the time delay between the two sources as well as their polarizations allows us to obtain a more detailed understanding of the DI mechanism.

[a)]Author to whom correspondence should be addressed. Electronic mail: mkawasa7@ip.media.kyoto-u.ac.jp
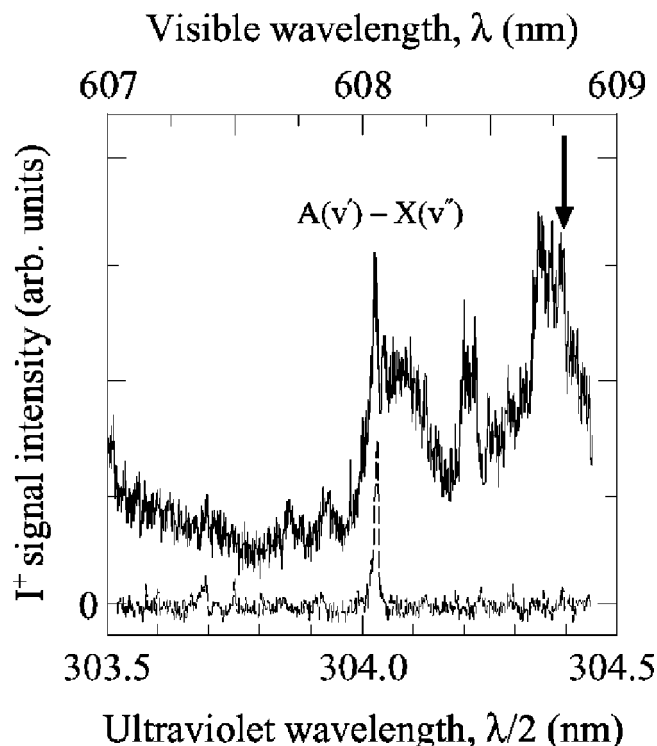[b)]Electronic mail: rjgordon@uic.edu

FIG. 1. The I^+ spectra from ICl in the two-color experiment with nonresonant ultraviolet plus visible laser light (solid curve) and in the one-color experiment with ultraviolet laser radiation only (broken curve). Vibrational assignments for the $A\,^3\Pi_1(v') \leftarrow X\,^1\Sigma^+(v'')$ transitions of $I^{35}Cl$ and $I^{37}Cl$ are discussed in Sec. IV C. The arrow indicates the wavelength at which the images shown in Fig. 4 were measured.

II. EXPERIMENT

We have used the velocity map imaging technique to measure both the speed and angular distributions of atomic iodine ions.[9,10] Linearly polarized UV and/or VIS lasers were used to irradiate a molecular beam of ICl seeded in 1 atm of Ar gas and pulsed at 10 Hz (General Valve, 0.8 mm orifice diameter). The VIS laser radiation near 608 nm and the UV radiation near 304 nm were provided by a Nd:YAG-pumped dye laser (Rhodamine B/Lambda Physik ScanMate 2EC, 6 ns pulse duration) and its second harmonic generated in a KDP crystal, respectively. Some additional measurements involving a one-color pump-and-probe scheme employed UV laser radiation at 304.02 nm, which was used both to photolyse the ICl molecules and also to probe the resulting $I^*(^2P_{1/2})$ fragment atoms by (2+1) resonance-enhanced multiphoton ionization (REMPI). In the time-delay experiments, the second and third harmonics of a Nd:YAG laser (Spectra Physics, LAB-130, 5–7 ns pulse duration, 10 Hz) provided radiation at 532 and 355 nm, respectively. The laser beam was focused with a 20 cm focal length lens into the reaction chamber. The pump and probe lasers were generally counter-propagated, except for the 304+608 nm experiments, where they were co-propagated. For each wavelength, the pulse energies measured before the lens were 0.5 and 15 mJ in the UV and VIS, respectively, unless otherwise noted. The delay time between two YAG laser pulses was controlled by a pulse generator (Stanford Research, DG535) and could be extended to as long as ± 2 μs with a jitter of a few ns. The molecular beam was directed along the axis of a 60 cm long Wiley-McLaren time-of-flight mass spectrometer operated under velocity-sensitive conditions.[9] The skimmed molecular beam source, the ionization chamber, and the flight tube were each differentially pumped.

The laser beams were linearly polarized perpendicular and/or parallel to the flight axis and focused onto the molecular beam between the repeller and extractor electrodes. Ions were accelerated by an electrostatic lens and focused onto a microchannel plate (MCP) detector mounted at the end of the flight tube. The electrode voltages were typically 2.5 kV for the repeller and 1.7 kV for the extractor. Typical voltages used for the MCP were 0 V (front face) and 1.2 kV (rear of the MCP pair), with 3.3 kV applied to the phosphor screen. The image produced on the phosphor screen by each laser shot was captured by a frame grabber connected to a CCD camera with a time-gated image intensifier (Hamamatsu, C4347) and accumulated in a laboratory computer. Typically, 20 000 laser shots were summed to produce a single two-dimensional (2-D) map of the transverse recoil velocity of the I^+ ions (selected by appropriate choice of time gate on the image intensifier). The images of the full three-dimensional velocity distribution were calculated from the 2-D maps by an inversion procedure developed by Matsumi et al.[11]

III. RESULTS

A. Excitation spectra of I^+ in one- and two-color experiments

Figure 1 shows the I^+ excitation spectrum of ICl in the two-color experiments using VIS laser light scanned from $\lambda=607$ to 609 nm and its second harmonic, $\lambda/2=303.5$ to 304.5 nm (solid curve). The time delay, Δt, between the VIS (λ) and UV ($\lambda/2$) beams was zero in this case. The solid curve shows the integrated I^+ signal intensity, i.e., the appropriate time-gated total current from the MCP, which was monitored as a function of the laser wavelength. The dashed curve in Fig. 1 shows the I^+ spectrum obtained in the one-color UV experiment, in which the two sharp resonances are due to the (2+1) REMPI of I^* ($^2P_{1/2}$) and $I(^2P_{3/2})$ atoms produced by one-photon UV dissociation of ICl.[12] The two-color spectrum of I^+ clearly shows the two-photon resonances at 304.02 and 303.69 nm evident in the one-color experiment, superimposed on a continuous broad background. At this UV intensity, no I^+ signal was observed in the one-color experiment when the UV radiation was tuned off-resonance.

Figure 2 shows I^+ excitation spectra in two-color experiments with different combinations of VIS and UV laser wavelengths. Figure 2(a) was obtained by scanning the VIS wavelength, λ, with the UV radiation fixed at 355 nm, whereas Fig. 2(b) was obtained by scanning the UV wavelength, $\lambda/2$, with the VIS radiation fixed at 532 nm. In both spectra Δt was set at zero. The nonresonant two-color I^+ spectrum in Fig. 2(a) shows a broad feature for $\lambda>608$ nm, whereas Fig. 2(b) shows four sharp peaks that are due to (2+1) REMPI of I and I* produced by one-photon dissociation of ICl. The transitions of these REMPI peaks are given
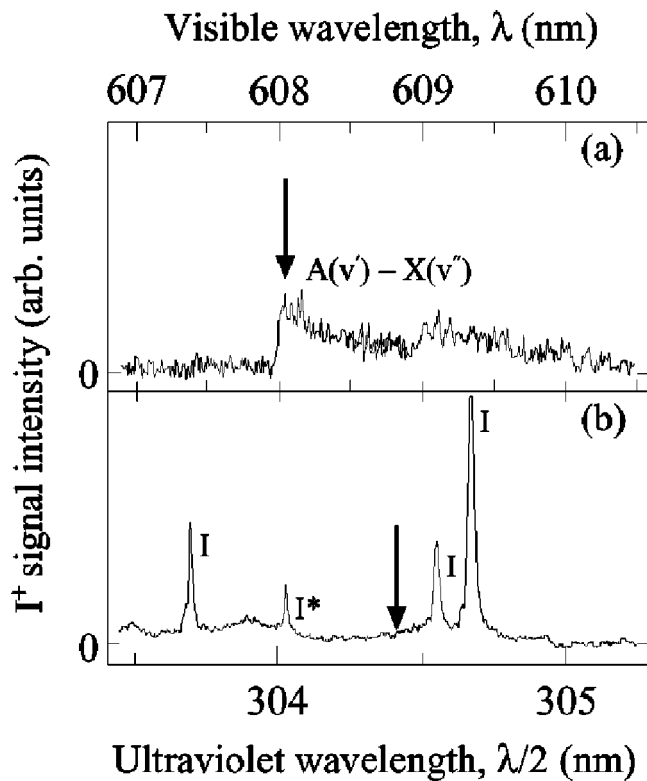
京都大学
KYOTO UNIVERSITY

A Self-archived copy in
Kyoto University Research Information Repository
https://repository.kulib.kyoto-u.ac.jp

京都大学学術情報リポジトリ
KURENAI 紅
Kyoto University Research Information Repository

1132   J. Chem. Phys., Vol. 117, No. 3, 15 July 2002   Yamada *et al.*

FIG. 2. The I^+ spectra from ICl in the two-color experiments, with (a) the ultraviolet (UV) wavelength fixed at 355 nm while the visible wavelength was scanned, and with (b) the visible wavelength fixed at 532 nm and UV wavelength scanned. Vibrational assignments for the $A\,^3\Pi_1(v')$ $\leftarrow X\,^1\Sigma^+(v'')$ transitions of $I^{35}Cl$ and $I^{37}Cl$ are discussed in Sec. IV C. The arrows indicate the wavelength at which the images shown in Fig. 6(a) were measured. I and I* denote the UV two-photon resonance-enhanced multiphoton signals for $I(^2P_{3/2})$ and $I(^2P_{1/2})$, respectively. Assignments of these transitions are given in Ref. 12.

by Jung *et al.*[12] Importantly, under the all our experimental conditions, no I^+ signal was observed at any wavelength when the UV radiation (355 nm or $\lambda/2$) was absent.

B. 2-D velocity imaging maps and the kinetic energy distributions of I^+ photofragments near 304 nm, with and without 608 nm radiation

Figure 3 shows I^+ images obtained at 304.02 nm with only UV radiation present, corresponding to the sharp feature shown by the broken curve in Fig. 1. This image resulted from (2+1) REMPI of I* atoms produced by one-photon UV photodissociation of ICl. The single discrete ring displayed in Fig. 3 is explained by a single-photon dissociation mechanism, as discussed in Sec. IV B. Figure 4 shows I^+ images corresponding to the broad feature in the solid curve of Fig. 1, produced with both UV ($\lambda/2=304.40$ nm) and VIS (λ =608.80 nm, 12 mJ/pulse) radiation. Seen here is a central feature not present in the single-color image of Fig. 3. Both the central feature and the faint outer ring are produced by a DI process, as explained in Sec. IV B. The images in the various panels of Fig. 4 were taken with different polarization geometries. In the upper panels of Fig. 4, the UV polarization vector, E_{UV}, was aligned parallel to the flight axis, whereas in the middle panels it was perpendicular to the axis. The polarization vector of the VIS radiation, E_{VIS}, was per-
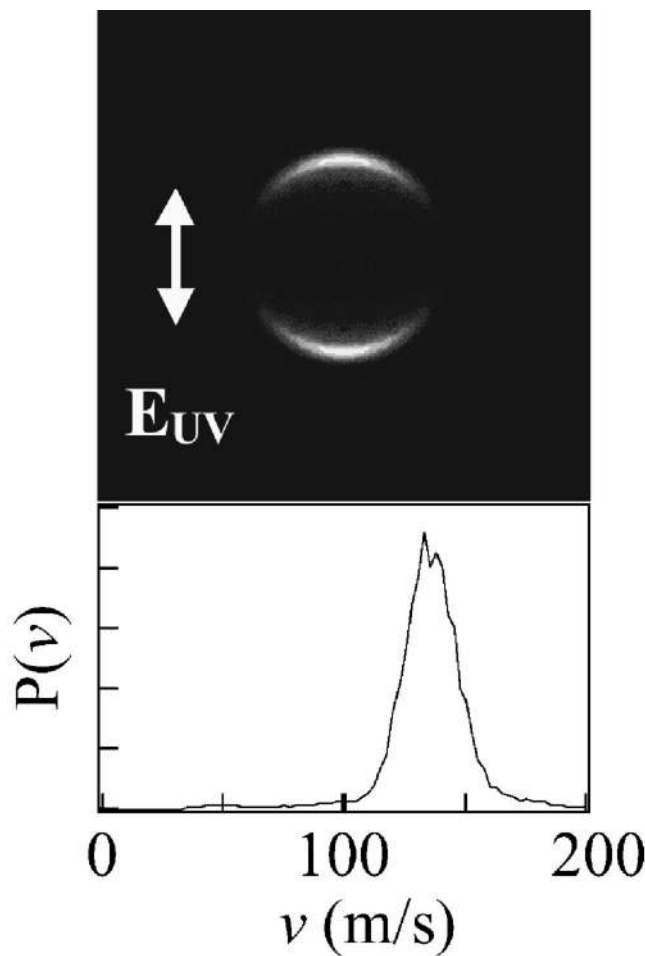

FIG. 3. Two-dimensional (2-D) images of the I^+ ions obtained from ICl by resonant one-color excitation at 304.02 nm, using the second harmonic of a dye laser tuned to a (2+1) REMPI transition of $I*(^2P_{1/2})$. The image was taken with the ultraviolet polarization (E_{UV}) aligned perpendicular to the detection axis. The lower panel shows the velocity distribution of $I*(^2P_{1/2})$ calculated from the upper image.

pendicular to the flight axis in the left images of Fig. 4 and parallel to the axis in the right images. It is apparent that the properties of the images are very sensitive to the alignment of E_{UV} and insensitive to E_{VIS}.

The images in Fig. 3 and the middle panels of Fig. 4 are all anisotropic. The angular distributions are fitted well by a Legendre series truncated after the second term,

$$I(\theta) \propto 1 + \beta P_2(\cos\theta), \tag{5}$$

where $I(\theta)$ is the normalized intensity of the photofragment, θ is the angle between the velocity of the fragment and the electric vector of the dissociation laser beam, and β is the one-photon angular anisotropy parameter. The fitted values of β are plotted in Fig. 5(a). The β value derived for the ring in Fig. 3 has the limiting value of 2, and those in Fig. 4 are approximately 0.7.

The center-of-mass translational energy distribution derived from the I^+ images shown in Figs. 3 and 4 are displayed in Fig. 5(b). The peaks labeled A and B in Fig. 5 correspond to the main features evident in the resonant one-color ion image and the two-color, off-resonance image (Figs. 3 and 4), respectively. The kinetic energy distribution
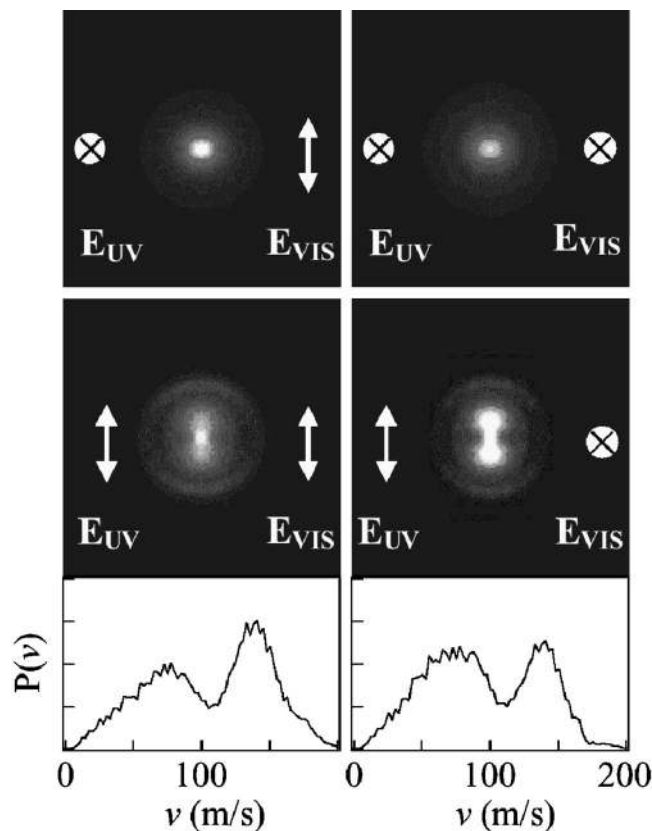
J. Chem. Phys., Vol. 117, No. 3, 15 July 2002

Ionization of ICl imaging spectroscopy   1133

FIG. 4. Two-dimensional (2-D) images of the I^+ ions obtained from ICl in the nonresonant two-color experiments using wavelengths of 304.40 and 608.80 nm. The image was taken with the ultraviolet polarization (E_{UV}) aligned parallel (upper panel) and perpendicular (middle panel) to the detection axis, respectively. The polarization vector of the visible laser light (E_{VIS}) is perpendicular and parallel to the detection axis in both images on the left and right sides, respectively. The lower panels show the velocity distributions of I* calculated from the middle images.

FIG. 5. (a) The angular anisotropy parameter (β) and (b) the c.m. translational energy distributions of the I* photofragment extracted from the images of Figs. 3 and 4 (left). In panel (a), the open squares (A) were obtained by one-color ultraviolet photodissociation to yield Cl+I*($^2P_{1/2}$), using the second harmonic of a dye laser tuned to the 2+1 REMPI transition of I*($^2P_{1/2}$) at 304.02 nm, whereas the filled squares (B) were obtained by two-color dissociative ionization to yield I*+Cl+e^-, using 304.40 and 608.80 nm. The distributions shown in panel (b) correspond to (A) one-color experiments at 304.02 nm (thin curve) and to (B) two-color experiments at 304.40 and 608.80 nm (thick curve), respectively. The arrows indicate the maximum available kinetic energies for each dissociation channel of ICl into I*($^3P_{0,1,2}$)+Cl(^2P), induced by absorption of three ultraviolet photons and one visible photon.

of the I^+ fragments obtained with the UV laser only, tuned to the two-photon resonance of I* (Fig. 3), shows a sharp peak centered at 22.2 kcal/mol displayed in Fig. 5(b) A.

The images obtained in the two-color nonresonant experiment (Fig. 4) display an outer ring and a central peak. The ratio of the integrated I^+ relative intensity of the outer ring to that of the central peak in the two-color nonresonant experiments was found to be independent of UV pulse energy between 0.5 and 3.5 mJ/pulse at 304.40 nm, with the 608.80 nm pulse energy fixed at 12 mJ/pulse.

C. 2-D velocity imaging maps of I^+ from two-color experiments with 355+608 nm and 304+532 nm

Figures 6(a) and 6(b) show the velocity image maps obtained with two different sets of UV and VIS wavelengths, namely (a) 355+608.04 nm and (b) 304.40+532 nm. Images were taken with both sets of wavelengths with E_{UV} aligned either parallel (upper panels) or perpendicular (lower panels) to the flight axis. In these images Δt was set at zero. As in the 304+608 nm experiment discussed previously (Fig. 4), the images were very sensitive to the alignment of E_{UV} and independent of that of E_{VIS}. (The effect of varying E_{VIS}
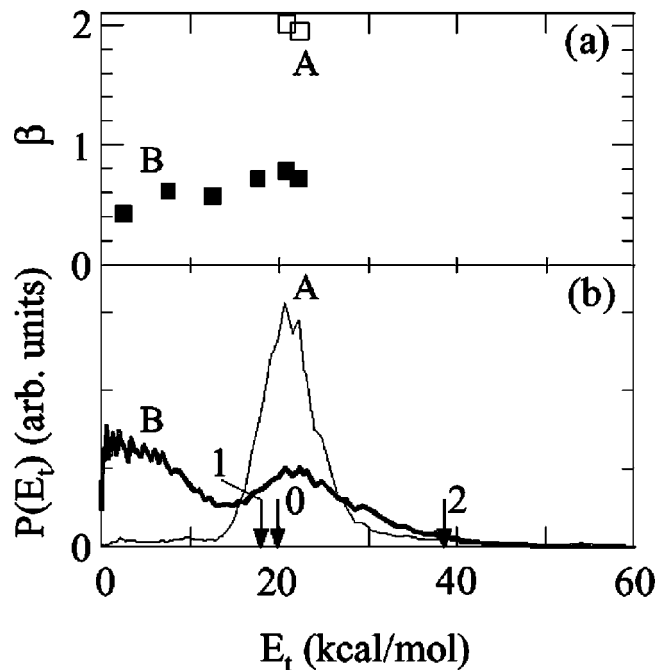
polarization is not shown in Fig. 6.) The peak translational energy calculated from the velocity distribution is as small as 2.0 kcal/mol for 355+608.04 nm.

D. Time-delay experiments

Figure 7 shows the integrated I^+ signal intensity versus Δt in the two-color experiments. Panel (a) corresponds to 355+608.04 nm, and panel (b) corresponds to 304.40+532 nm. A negative time delay in these figures means that the VIS pulse precedes the UV pulse. Figure 7(a) shows that the I^+ signal intensity increases in this case with the delay between the VIS and US pulses, reaching an asymptotic value at long delays. In Fig. 7(b), however, the I^+ signal was observed only when the UV and VIS pulses were temporarily overlapped within 10 ns.

IV. DISCUSSION

Our previous studies identified several identifying characteristics of dissociative ionization.[3,4] These include (1) the production of ionic fragments with nonresonant radiation and the appearance of fragment ions with kinetic energy distributions that are (2) continuous, (3) peaked near zero, and (4) have maxima that are independent of the excitation energy. A further property of multiphoton DI is (5) the involvement of
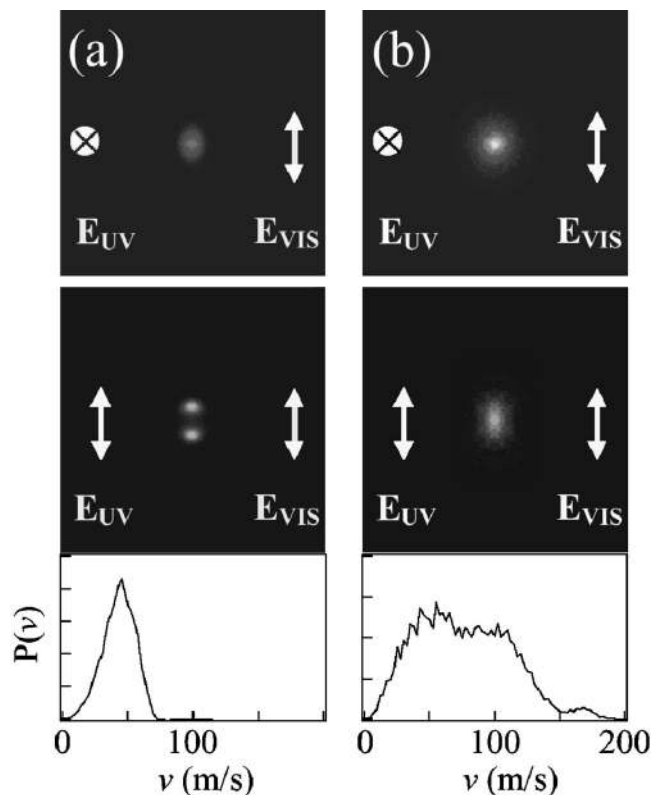
FIG. 6. Two-dimensional (2-D) images of the I^+ ions obtained from ICl with nonresonant two-color radiation, using wavelengths of (a) 355 and 608.04 nm and (b) 304.40 and 532 nm. The ultraviolet polarization (E_{UV}) was aligned either parallel (upper two panels) or perpendicular (middle panels) to the detection axis. The polarization vector of the visible laser light (E_{VIS}) was perpendicular to the detection axis in all images. The lower panels show the velocity distribution of I* calculated from the middle images.

FIG. 7. Time-resolved I^+ signal intensity produced from ICl with nonresonant two-color radiation using wavelengths of (a) 355 and 608.04 nm and (b) 304.40 and 532 nm. The horizontal axis is the delay time between the visible and ultraviolet laser pulses, where a negative delay time means that the visible pulse precedes the ultraviolet pulse.

intermediate gateway states that access the superexcited DI states. For diatomic molecules, property (2) necessarily implies that a third body (i.e., an electron) carries away a continuous amount of energy. Property (4) is also indicative of a continuous sink for energy. The present article reveals the presence of several of these effects in ICl, and, in particular, explores the role of intermediate states in property (5).

The outline of this discussion is as follows: In Sec. A we briefly review the electronic properties of ICl that are relevant to this study. In Sec. B we interpret the data obtained at 304+608 nm in light of a DI mechanism. Similarities and differences observed at 355+608 and 304+532 nm are explored in Secs. C and D.

A. Electronic properties of ICl

The visible absorption spectrum of ICl contains many closely spaced bands assigned to transitions to the $A\,^3\Pi_1$ (565–700 nm),[13] $B\,^3\Pi_{0^+}$ (562–576 nm),[14] and $B'\,^3\Pi_{0^+}$ (566–571 nm) states.[14] A continuum band between 370 and 550 nm is assigned to dissociation via the B state, and a second continuum between 220 and 300 nm is assigned to dissociation via higher $\Omega = 0^+$ and 1 states.[15,16]

The photodissociation dynamics of ICl have been investigated by state-selective photofragment translational spectroscopy at various wavelengths between 235 and 248 nm,[16]
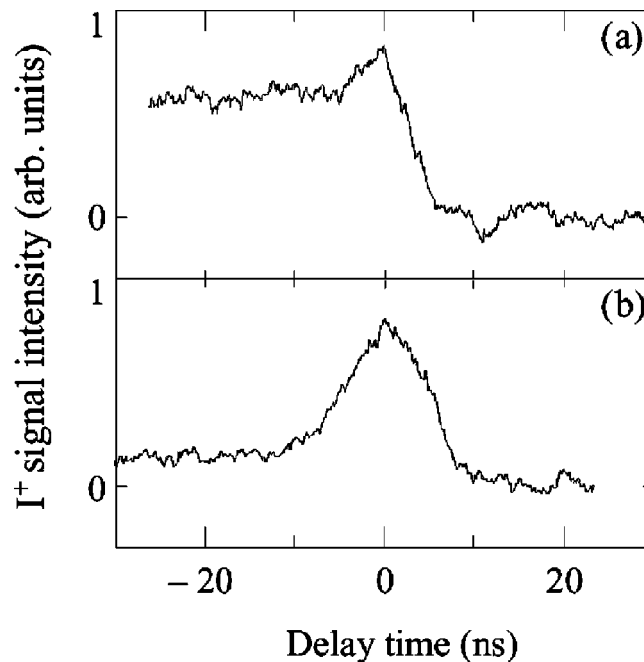
at 304 nm,[17] and in the 490–590 nm region.[18,19] In particular, the branching ratio and angular anisotropies of ground state and spin orbit-excited I and Cl were measured.

Yabushita and co-workers[16,20] calculated the adiabatic potential energy curves for the ground and first few excited states of ICl. Some of the relevant states and their diabatic dissociation products are shown schematically in Fig. 8. A high-resolution threshold photoelectron spectroscopic study
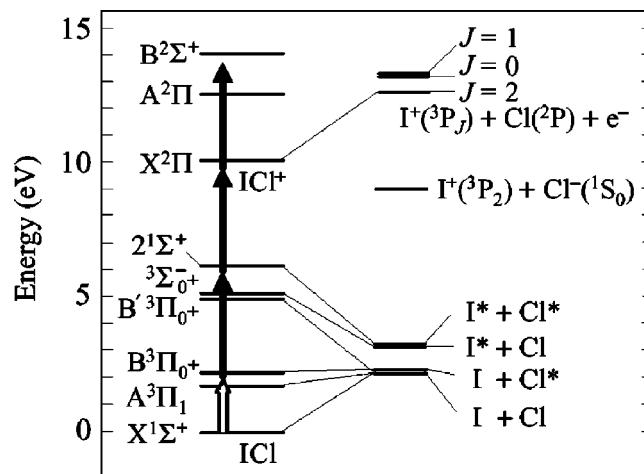

FIG. 8. Diabatic correlation diagram for possible dissociative ionization mechanisms of ICl (after Refs. 16, 17, 20, and 21). Not shown are several $\Omega=1$ states lying above the $A\,^3\Pi_1$ state. The solid arrows indicate the transition induced by the ultraviolet laser, and the open arrow shows the transition induced by the visible laser. The bound and repulsive states excited by the visible photon are the gateway for excitation by the UV photons to the upper electronic states. The symbols I, I*, Cl and Cl* denote the fragments $I(^2P_{3/2})$, $I(^2P_{1/2})$, $Cl(^2P_{3/2})$, and $Cl(^2P_{1/2})$, respectively.

of ICl above the valence ionization region was performed using synchrotron radiation.[21] The adiabatic ($v^+ = 0$) ionization potentials for formation of the $X\,^2\Pi_{3/2}$, $A\,^2\Pi$ and $B\,^2\Pi^+$ states of the ICl$^+$ ions are 10.076 ± 0.002, 12.5, and ~ 14 eV, respectively. (See Fig. 8.) The dissociation limit for $I^+(^3P_2) + Cl(^2P_{3/2})$ is 12.604 eV. The formation of the higher spin-orbit states of $I^+(^3P_J)$ needs an excess energy of 0.88 eV for $J=1$ and 0.80 eV for $J=0$, respectively. Extended vibrational structures seen in the photoelectron spectra for both the X and A band systems were assigned to resonant autoionization of Rydberg states and also to ion-pair states, especially in the energy region of the A state of ICl$^+$. In the present study, the DI process can occur through these excitation processes.

B. 304 and 608 nm

The discrete ring observed in the one-color image (Fig. 3) and the partially resolved double peaks at 20.7 and 22.2 kcal/mol in the recoil energy distribution [curve A in Fig. 5(b)] were obtained with the UV radiation tuned to an iodine resonance. These features correspond to the peaks reported previously by Jung et al.[17] at 20.0 and 22.0 kcal/mol, and are attributable to one-photon dissociation of ICl at 304.02 nm to produce I*+Cl* and I*+Cl fragments, followed by (2+1) REMPI of the I* atoms,

$$ICl + h\nu(\text{UV}) \rightarrow I^* + Cl/I^* + Cl^*, \tag{6a}$$

$$I^* + 3h\upsilon(\text{UV}) \rightarrow I^+ + e^-. \tag{6b}$$

The β value for the ring in Fig. 3 has the limiting value of 2, which indicates a parallel electronic transition ($\Delta\Omega = 0$). This finding is consistent with a transition from the $X^1\Sigma^+$ (2440) ground state of ICl to primarily the $B'\,^3\Pi_{0^+}$. (2341) state, followed by a nonadiabatic transition to the $^3\Sigma_{0^+}^-$ (2422) state to form I*+Cl products.[17,22] (As shown in Fig. 8, the diabatic products of the $^3\Sigma_{0^+}^-$ states are I*+Cl, whereas those of the $2^1\Sigma^+$ state are I*+Cl*.)

The two-color images shown in Fig. 4 were obtained with the UV radiation tuned off-resonance. The outer ring in these images is not attributable to nonresonant multiphoton ionization of I* by UV (304.40 nm) laser light [produced by reaction (6a)], even though it has nearly the same energy as that in Fig. 3, because the dashed curve in Fig. 1 shows no I$^+$ signal produced by *nonresonant* UV radiation, and also because its β value of 0.7 is much smaller than the limiting value of 2 observed for resonant excitation.
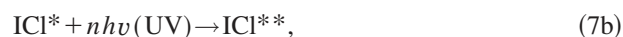
The velocity map images of I* ions produced by off-resonant two-color irradiation of ICl at 304.40 and 608.80 nm display an intense central feature (Fig. 4), which is explained by a DI mechanism. In a DI process, the electron can carry away a continuous amount of kinetic energy, so that the recoiling ion-neutral pair displays a continuous distribution of kinetic energies that may be peaked near zero. The central feature observed in the I$^+$ images of Fig. 4 resembles those observed in earlier studies of DI.[3–6,23,24] Previously it was proposed that DI mechanisms contribute to the photoinduced dynamics of I$_2$,[3] C$_6$H$_5$I,[4] NO$_2$,[6] CF$_3$I,[7] C$_3$H$_8$,[23] and D$_2$.[24] In the absence of collisions and dressed state effects, continuous structure in the fragment recoil kinetic energy distribu-

tions *for a diatomic molecule* can arise *only* if a third body (i.e., an electron) carried away the excess energy.

Dissociative ionization occurs when a molecule is excited to a superexcited neutral state that can decay either by dissociating into excited neutral fragments or by autoionizing to a dissociative ionic state. The distribution of kinetic energies of the recoiling nuclei is determined by the competition between ionization and dissociation. The distribution may be peaked near zero kinetic energy if the dissociative ionic state is less repulsive than the superexcited neutral state. (See Fig. 4 of Ref. 3.) If the molecule autoionizes near the repulsive wall of the neutral state, where the nuclear kinetic energy is zero and the transition moment is likely to be large, then the electron will carry away most of the available energy and angular momentum. The longer the molecule survives in the neutral state, the greater the amount of potential energy that is converted into nuclear recoil energy. The detailed shape of the kinetic energy distribution function is determined by the neutral and ionic potential energy curves and by the radial dependence of the transition moment.

Both the central feature and the outer ring are explained by DI processes. The low energy peak is attributed to dissociation of the molecular ion on a weakly bound potential energy curve, whereas the outer ring may be explained by direct ionization on a repulsive ionic curve. Both mechanisms were observed for the I$_2$ molecule. (See Fig. 4 of Ref. 3.) Strong evidence for the mechanism producing the discrete ring in I$_2$ is that the recoil energy of the rings varied very weakly with photon energy. A similar mechanism may also be responsible for the outer ring observed for iodobenzene.[4]

Clearly, a key step in DI is the transition to the superexcited state, AB^{**} in reaction (1). For single-photon excitation, the transition probability is determined by the electronic transition dipole moment and the Franck–Condon overlap integral. For multiphoton excitation, however, the mechanism may be complicated by the presence of intermediate electronic states. The present experiments demonstrate that a transition to such a gateway state, AB^*, induced by absorption of one VIS photon, is a necessary condition for DI of ICl. The transition from the gateway to the superexcited state is induced by absorption of several UV photons, and the angular distribution of the nuclear fragments is determined by the polarization vector of the UV laser. The overall proposed mechanism is therefore as follows:

$$ICl + h\upsilon(\text{VIS}) \rightarrow ICl^*, \tag{7a}$$

$$ICl^* + nh\upsilon(\text{UV}) \rightarrow ICl^{**}, \tag{7b}$$

$$ICl^{**} \rightarrow ICl^{+*} + e^-, \tag{7c}$$

$$ICl^{+*} \rightarrow I^+ + Cl. \tag{7d}$$

As discussed in the following section, a plausible candidate for ICl* in step (7a) is the $A\,^3\Pi_1$ state. In our experiment, the energy required for step (7b) corresponds to $n=3$. Potential energy is removed from the nuclei in step (7c), and nuclear recoil energy is released in step (7d). The $A\,^2\Pi$ and $B\,^2\Sigma^+$ states of ICl$^+$ are possible candidates for ICl^{+*}, as shown in Fig. 8.

The total energy, E_{avl}, available to the recoiling nuclei in the overall process

$$ICl + hv(VIS) + 3h(UV) \rightarrow I^+(^3P_j) + Cl + e^- \qquad (8)$$
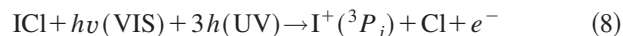
may be calculated from the dissociation energy[17] of ICl and the ionization potential of $I(^2P_{3/2})$. For 304.40+608.80 nm, $E_{avl} = 38.2$ kcal/mol for $J=2$, 19.7 kcal/mol for $J=0$, and 17.9 kcal/mol for $J=1$. The formation of three different J states of $I^+(^3P_j)$ can explain the observed kinetic energy distribution shown in Fig. 5(b) B, where the maximum available translational energies for the three J levels are indicated by the arrows. The translational energy distribution of I^+ is consistent with these threshold energies, suggesting that at least two different J states of $I^+(^3P_j)$ are formed. The maximum observed kinetic energy exceeds the available energy for $J=2$ by ~ 2 kcal/mol, suggesting a hot-band mechanism from ICl $(X^1\Sigma^+, v''=2, E_v=2.2$ kcal/mol). The population of $v''=2$ at room temperature is 2.5%, and hot bands of ICl were in fact observed in the photoelectron spectra reported by Yencha *et al.*[21] and in the absorption spectra reported by Hulthén *et al.*[14]
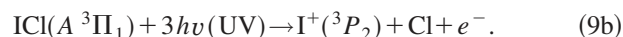
The angular distribution of I^+ is well represented by Eq. (5) with only the P_2 term included in the series. It is well known that for an n-photon photodissociation with no bound intermediate states, the angular distribution includes even order Legendre polynomials up to order $2n$.[4,25,26] Here, the absence of terms higher than $n=2$ could be explained if the three-photon dissociation of ICl* involves a bound intermediate state, so that the anisotropy is determined entirely by the last photon to be absorbed.[25] Possible explanations of the small β values [$\beta \cong 0.7$ in Fig. 5(a) B] include (a) a long dissociative lifetime of ICl^{+*} in step (7d), (b) mixing of several excited electronic states with different symmetries in step (7d), caused by strong nonadiabatic interactions of the accessible states, and (c) removal of angular momentum by the electron emitted in step (7c). Mechanism (a) is possible if the potential energy curve for ICl^{+*} is flat or weakly bound. In the latter case, ICl^{+*} must be initially formed with sufficient energy to dissociate. Mechanism (b) is possible because there exist as many as five possible final ionic states $(X^2\Pi_{1/2,3/2}, A^2\Pi_{1/2,3/2}, $ and $B^2\Sigma^+)$.[21] Mechanism (c) is plausible because angular momentum carried away by the electron reduces the angular anisotropy of the recoiling nuclei. This is true especially for p- or d-wave electrons, which remove most of the angular momentum supplied by the photon. In the case of H_2 photoionization, where the intermediate rovibrational level is completely defined, Bakker *et al.*[5] were able to calculate the expected β value using angular momentum algebra. In the present case, where the electronic character and rotational angular momentum of the intermediate states are not well defined and their coupling matrix elements are unknown, such a calculation would be much more difficult.

We note that ion-pair states, analogous to zero kinetic energy electron (ZEKE) Rydberg states, could conceivably be responsible for the features seen in our images. Such ion-pair states have recently been observed in a multiphoton spectrum of ICl between 8.99 and 9.08 eV in the presence of a 1.25 kV/cm dc field.[1] The asymptotic dissociation limit is 8.98 eV for the ion-pair state, $I^+ + Cl^-$. For the 304.40 +608.80 nm experiment, however, a sharp peak corresponding to the total translational energy of 28 kcal/mol is absent in Fig. 5(b) B. Likewise, the asymptotic dissociation limit is 12.1 eV for the ion-pair state, $I^- + Cl^+$. Our failure to observe a Cl^+ signal is a further indication that the ion-pair state is not formed.

C. 355+608 nm

The velocity map image of I^+ ions produced by two-color irradiation of ICl at 355+608.04 nm displays only a central anisotropic feature, shown in the middle panel of Fig. 6(a). This feature corresponds to a translational energy distribution peaked at 2.0 kcal/mol. The I^+ ion images shown in Fig. 6(a) are found to depend on the alignment of $\mathbf{E}_{UV}$, in good agreement with the observations for 304.40+608.80 nm excitation. In the time-delay experiment, the I^+ signal for 355+608.04 nm is observed only when the VIS pulse precedes the UV pulse [Fig. 7(a)]. This effect is attributed to a transition to a bound gateway state of ICl with one VIS photon [reaction (7a)]. An ICl molecule in the bound gateway state is then ionized by absorption of several UV photons. We note that the threshold for dissociation of ICl to ground state atoms is 576 nm. The $A^3\Pi_1$ state of ICl, however, is accessible by a one-photon transition with VIS laser light around 608 nm,[20]

$$ICl(X^1\Sigma^+) + hv(VIS) \rightarrow ICl(A^3\Pi_1), \qquad (9a)$$

$$ICl(A^3\Pi_1) + 3hv(UV) \rightarrow I^+(^3P_2) + Cl + e^-. \qquad (9b)$$

For 355+608 nm, this reaction is endoergic by 2 kcal/mol. As before, the energy defect may be explained by the presence of vibrationally excited molecules in the molecular beam.

The nonresonant two-color I^+ spectrum in Fig. 2(a) shows a broad feature for $\lambda > 608$ nm, which is similar to the structure observed near 608 nm in the two-color spectrum of I^+ shown in Fig. 1 (solid line). The similarity of these spectra suggests that the feature near 608 nm in Fig. 1 is produced by the absorption of a VIS photon. These features in Figs. 1 and 2(a) are assigned to four overlapping transitions peaked at 608 nm, $A(^3\Pi_1, v') \leftarrow X(^1\Sigma^+, v'')$ with $(v', v'') = (17,0),(21,1),(28,2)$ for $I^{35}Cl$ and $(28,2)$ for $I^{37}Cl$. The peak at 609 nm may be assigned to the transition $A(^3\Pi_1, v'=21) \leftarrow X(^1\Sigma^+, v''=1)$ for $I^{37}Cl$. The transition energies were calculated using the isotopic term values for the A state listed in Ref. 14 and the molecular constants of the X state listed in Ref. 27. Because vibrational cooling in a jet expansion is much less efficient than rotational cooling, the vibrationally excited ICl may survive in the free jet while the rotational temperature is very low.[28] The photodissociation mechanism in Eq. (9) is energetically accessible for a hot-band transition from $ICl(X^1\Sigma^+, v''=2, E_v = 2.2$ kcal/mol).

The structures around 607.9–608.3 nm shown in Fig. 1 (solid line) correspond to the rotational population of ICl $(X^1\Sigma^+, v''=0,1,2,J'')$ with a Boltzmann temperature of ~ 20 K. These features are the signature of the gateway transitions present in the two-color DI mechanism. On the other hand,

some of the structures overlapping the continuum band around 608.3–608.9 nm in Fig. 1 (solid line) are not seen in Fig. 2(a) and cannot be assigned to the $A-X$ transition. Those structures should be independent of the wavelength of the VIS photon and thus reflect the transition from ICl(A) to a higher electronic state induced by the UV photons.

This proposed mechanism is consistent with all of the experimental observations. For example, without VIS laser light, no I$^+$ signal was observed. As shown in Fig. 6(a),the angular distributions of I$^+$ depend sensitively on the direction of $\mathbf{E}_{UV}$, but not of $\mathbf{E}_{VIS}$. [The effect of varying $\mathbf{E}_{VIS}$ polarization is not shown in Fig. 6(a).] The two-color experiments with 304+608 nm and 355+608 nm utilize the same VIS laser wavelength and thus access the same gateway state of ICl. We therefore expect that the results of the time-delay experiment performed for 355+608.04 nm should apply to 304.40+608.80 nm as well. We note that the outer ring present at 304+608 nm is absent at 355+608 nm. In the former case we argued that the outer ring is caused by direct DI on a repulsive ionic curve, which is clearly the case for I$_2$.[3] The absence of the ring at 355+608 nm may be simply the result of a much weaker transition to this state at longer wavelengths. This mechanism may also explain the vanishing of the outer ring in iodobenzene as the wavelength is increased.[4]

It is instructive to compare our results with those reported by Parker *et al.*[29] for the single-color multiphoton dissociation and ionization of Cl$_2$. In their case a highly structured kinetic energy distribution was observed for both Cl$^+$ and e^-. Their proposed mechanism is a two-photon excitation of a discrete Rydberg state followed by one-photon excitation of the core to produce a superexcited neutral state, which either autoionizes to produce the molecular ion or dissociates to yield excited Cl atoms. The observed kinetic energy distribution of Cl$^+$ results form either photodissociation of Cl$_2^+$ or nonresonant ionization of excited Cl.

These observations are in striking contrast with the present results. The absence of structure in the recoil energy distribution of I$^+$ and the low peak energy are indicative of a DI mechanism. Although the time-delay experiment indicates that the intermediate state is long-lived, removal of a continuous amount of kinetic energy by the departing electron results in a structureless kinetic energy distribution for the ion.

D. 304+532 nm

Figure 6(b) shows the velocity image maps obtained in a two-color experiment with 304.40+532 nm. Again a central feature characteristic of a DI mechanism is present. As in the previous two-color experiments, the properties of the image are sensitive to the alignment of $\mathbf{E}_{UV}$ and are independent of $\mathbf{E}_{VIS}$. In the time-delay experiment, the central feature was observed only when the UV and VIS pulses were temporally overlapped within 10 ns, as shown in Fig. 7(b). This finding indicates that in this case DI of ICl utilizes an unbound gateway state. A single gateway, which explains both sets of time-delay data in Fig. 7, is the $A\,^3\Pi_1$ state. Below its dissociation threshold (2.153 eV, or 576 nm), the very long

lifetime of this state (100 μs at 607 nm)[30] explains the persistence of the DI signal when the VIS pulse arrives before the UV pulse, whereas its short lifetime above the dissociation threshold requires that the pulses be temporally overlapped.

A possible competing mechanism at these wavelengths is the 1VIS+2UV photoionization of ICl, followed by single-photon UV photodissociation of ICl$^+$. If this were the case, however, the translational energy of I$^+$ would be greater than 35 kcal/mol. The absence of such high energy ions indicates that this is not the main mechanism.

V. CONCLUSIONS

Velocity map imaging has been used to explore the photoexcitation dynamics of ICl induced by two-color radiation. Experiments were performed with three pairs of visible (VIS) and ultraviolet (UV) laser pulses (304+608 nm, 355+608 nm, and 304+532 nm). All the velocity map images of I$^+$ produced by nonresonant bichromatic excitation of ICl displayed a low velocity feature that is characteristic of a dissociative ionization (DI) mechanism.[3,4] Nonresonant photo-induced dynamics of ICl to form I$^+$ ions is thus shown to proceed via three-body DI processes, in which the electron carries off a continuous amount of kinetic energy. Time-delay measurements show that an intermediate gateway state (or states) resonant at the VIS photon energy enhances the DI processes. It is suggested that this gateway is the $A\,^3\Pi_1$ state, which is reached with a single VIS photon. Subsequent absorption of three UV photons leads to a superexcited DI state. The kinetic energy distribution of the recoiling nuclear fragments is determined by the competition between dissociation and autoionization of the DI state.

[1] S. Wang, K. P. Lawley, T. Ridley, and R. J. Donovan, Faraday Discuss. **115**, 345 (2000).
[2] I. Nenner and J. A. Beswick, in *Handbook of Synchrotron Radiation*, edited by G. V. Marr (Elsevier, Amsterdam, 1987), Vol. 2, pp. 355–466.
[3] S. Unny, Y. Du, L. Zhu, R. J. Gordon, A. Sugita, M. Kawasaki, Y. Matsumi, and T. Seideman, Phys. Rev. Lett. **86**, 2245 (2001).
[4] S. Unny, Y. Du, L. Zhu *et al.*, J. Phys. Chem. A **105**, 2270 (2001).
[5] B. L. G. Bakker, D. H. Parker, and W. J. van der Zande, Phys. Rev. Lett. **86**, 3272 (2001).
[6] J. A. Davies, J. E. LeClaire, R. E. Continetti, and C. C. Hayden, J. Chem. Phys. **111**, 1 (1999).
[7] W. G. Roeterdink and M. H. M. Janssen, Phys. Chem. Chem. Phys. **4**, 601 (2002).
[8] M. S. Child and R. B. Bernstein, J. Chem. Phys. **59**, 5916 (1973).
[9] A. T. J. B. Eppink and D. H. Parker, J. Chem. Phys. **109**, 4758 (1998).
[10] D. W. Chandler and P. L. Houston, J. Chem. Phys. **87**, 1445 (1987).
[11] Y. Sato, Y. Matsumi, M. Kawasaki, K. Tsukiyama, and R. Bersohn, J. Phys. Chem. **99**, 16307 (1995).

1138   J. Chem. Phys., Vol. 117, No. 3, 15 July 2002

Yamada *et al.*

[12] Y.-J. Jung, Y. S. Kim, W. K. Kang, and K.-H. Jung, J. Chem. Phys. **107**, 7187 (1997).

[13] E. Hulthén, N. Johansson, and U. Pilsäter, Ark. Fys. **14**, 31 (1958); **18**, 479 (1960).

[14] W. G. Brown and G. E. Gibson, Phys. Rev. **40**, 529 (1932).

[15] D. J. Seery and D. Britton, J. Phys. Chem. **68**, 2263 (1964).

[16] K. Tonokura, Y. Matsumi, M. Kawasaki, H. L. Kim, S. Yabushita, S. Fujimura, and K. Saito, J. Chem. Phys. **99**, 3461 (1993).

[17] K.-W. Jung, T. S. Ahmadi, and M. A. El-Sayed, J. Phys. Chem. A **101**, 6562 (1997).

[18] T. P. Rakitzis, S. A. Kandel, and R. N. Zare, J. Chem. Phys. **108**, 8291 (1998).

[19] T. P. Rakitzis, S. A. Kandel, A. J. Alexander, Z. H. Kim, and R. N. Zare, J. Chem. Phys. **110**, 3351 (1999).

[20] S. Yabushita, J. Mol. Struct.: THEOCHEM **461**, 523 (1999).

[21] A. J. Yencha, M. C. A. Loppes, and G. C. King, Chem. Phys. Lett. **325**, 559 (2000).

[22] The four integers given in parentheses correspond to Mulliken's notation for the electronic configuration $(\sigma, \pi, \pi^*, \sigma^*)$ after R. S. Mulliken, J. Chem. Phys. **55**, 288 (1971).

[23] T. Fiegele, C. Mair, P. Scheier, K. Becker, and T. D. Märk, Int. J. Mass. Spectrom. **207**, 145 (2001).

[24] K. Vijayalakshmi, A. Talebpour, T. T. Nguyen-Dang, J. Yang, A. D. Bandrauk, and S. L. Chin, Phys. Rev. A **62**, 053408 (2000).

[25] M. Kawasaki, H. Sato, T. Kikuchi, A. Fukuroda, H. Kobayashi, and T. Arikawa, J. Chem. Phys. **86**, 4425 (1987).

[26] R. J. Gordon and G. E. Hall, in Advanced Chemical Physics, Vol. XCVI, edited by I. Prigogine and S. A. Rice (Wiley, New York, 1996), pp. 1–50.

[27] K. P. Huber and G. Herzberg, *Molecular Spectra and Molecular Structure, IV. Constants of Diatomic Molecules* (Van Nostrand Reinhold, New York, 1979), p. 340.

[28] D. R. Miller, *Atomic and Molecular Beam Methods*, edited by G. Scoles (Oxford University Press, New York, 1988), Vol. 1, p. 14.

[29] D. H. Parker, B. L. G. Bakker, P. C. Samartzis, and T. N. Kitsopoulos, J. Chem. Phys. **115**, 1205 (2001).

[30] G. W. Holleman and J. I. Steinfeld, Chem. Phys. Lett. **12**, 431 (1971).